The Influence of Transformation Induced Plasticity on Damage Development in a Medium-Mn Third-Generation Advanced High Strength Steel

Concetta Pelligra[1], David S. Wilkinson[1], Joseph McDermid[1]
[1]Department of Materials Science and Engineering, McMaster University

Introduction

Considerable research has been invested in developing processing techniques to create Advanced High Strength Steels (AHSSs), and to stabilize critical phases at ambient temperatures; however, little has been done to determine the extent to which the stress-driven transformation from metastable retained austenite (RA) to martensite (M), Transformation Induced Plasticity (TRIP), can suppress or delay damage. The ability to tailor the stability of RA during deformation has been crucial in manipulating the strength to ductility ratio, and therefore TRIP kinetics of 3G Medium-Mn steels.

The iconic banana diagram offers limited information on the true capability of these steels to be formed into complex automotive components. Moreover, the reduction in area/true strain to fracture from a uniaxial tensile test, offers an alternative measure of ductility that can be correlated with various forming operations that involve bending[1] and Hance's diagram[2] is an alternative means of defining material ductility.

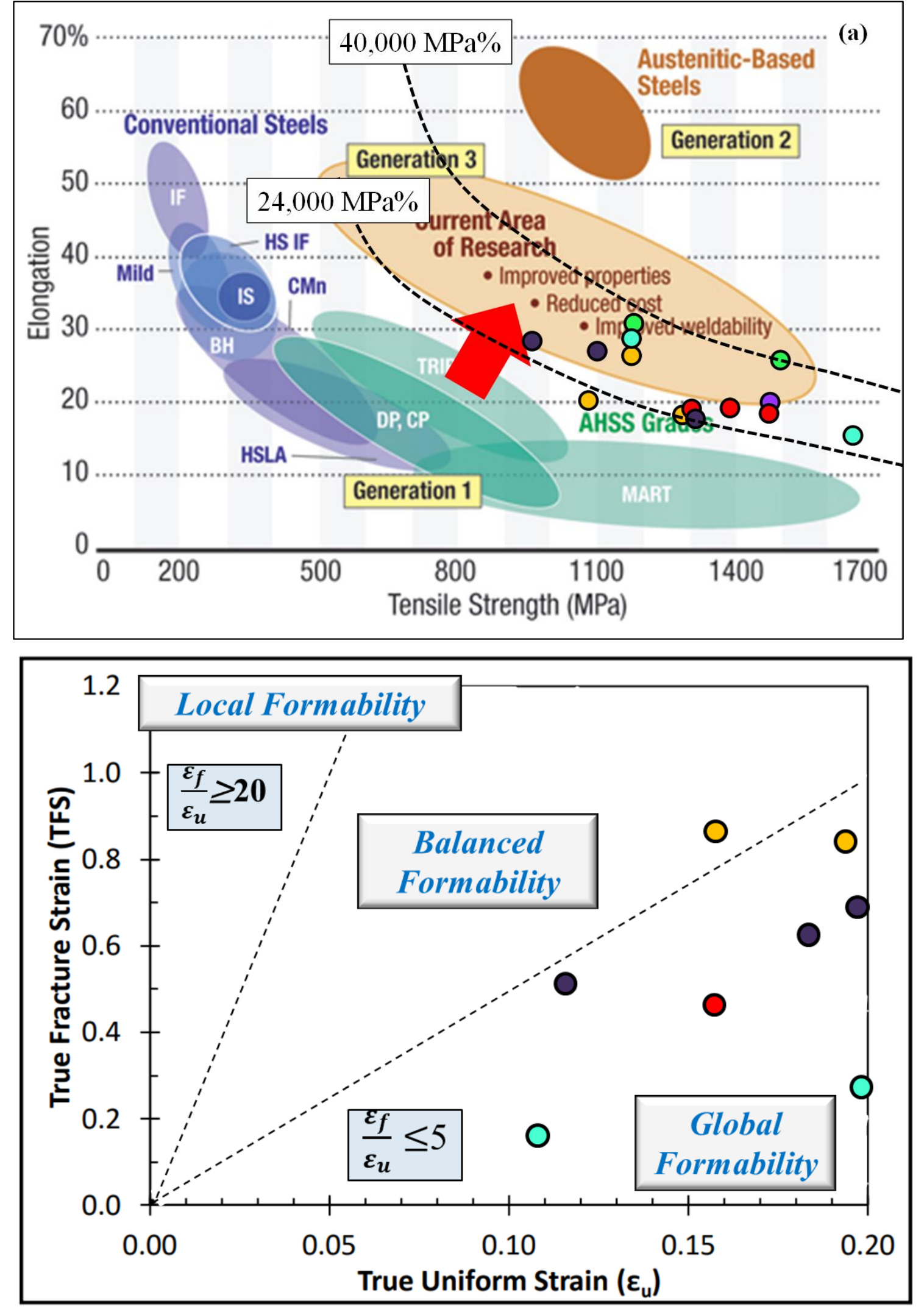

Medium Mn Steels			
🔴	Steel A (0.2C-6.3Mn-1.5Si-0.52Al)	🟢	Steel H (0.2C-6.2Mn-1.0Si-1.6Al)
🟡	Steel E (0.15C-6.0Mn-1.1Si-1.9Al)	🟣	Steel M (0.15C-5.8Mn-0.71Si-1.8Al)

Figure 1 (a) Banana Diagram (b) Hance's diagram with a series of plotted Medium-Mn steels

This work aims to determine the mechanisms that control the damage and fracture response of Medium-Mn steels and to thereby suggest approaches that will optimize TRIP kinetics, damage suppression and achieve 3G mechanical targets.

Objectives

<u>Overall:</u> Determine the intercritical annealing (IA) parameters that mitigates damage, and improves ductility through the use of an optimal TRIP rate in a prototype Medium-Mn steel

- **Determine the micro-mechanisms & quantify the amount of damage that contributes to overall fracture with modest adjustments in IA temperatures**
- **Determine the relationship between TRIP kinetics and damage**
- **Investigate the role of triaxiality on the TRIP-damage relationship**

M-MF-710 ºC-120s
M-MF-685 ºC-120s
M-MF-665 ºC-120s

Methodology

Pictorial representation of research methodology to determine the relationship between TRIP and damage using strain as the intermediate parameter.

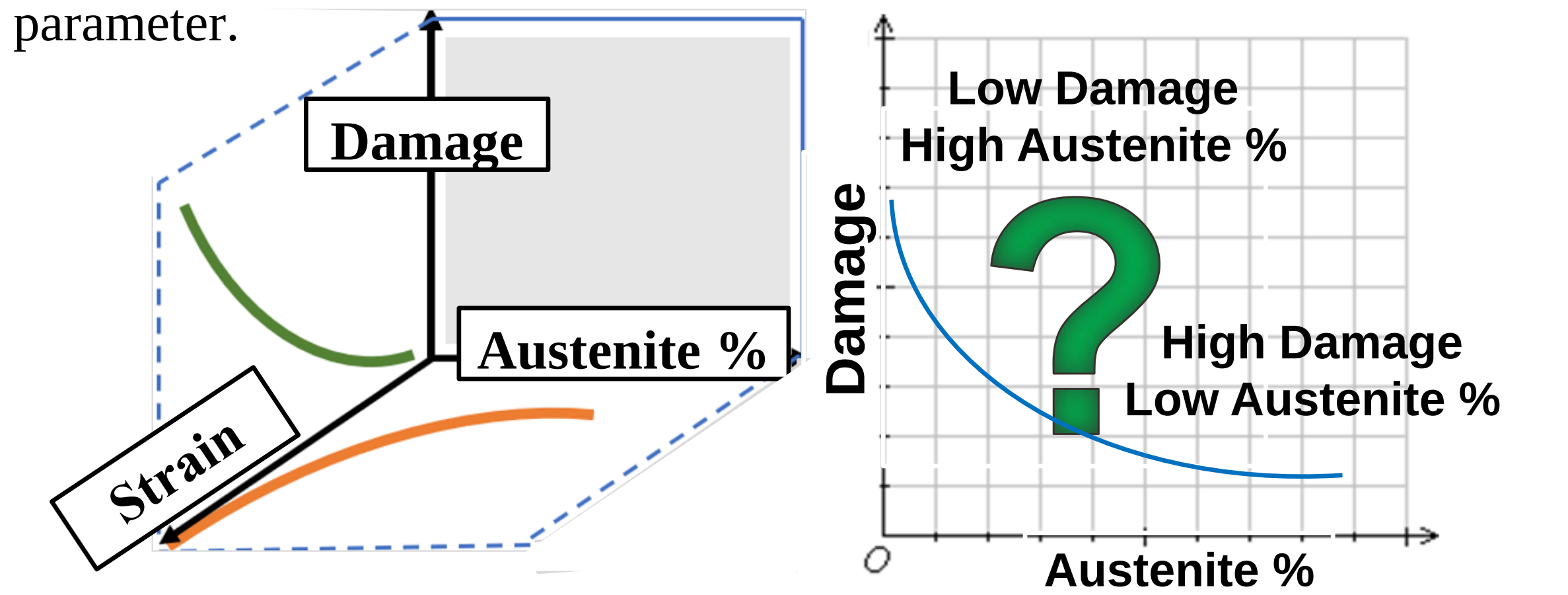

Figure 2 Research Methodology Schematic

Material

The alloy design was based on previous work showing that 0.2C-6Mn-(1-1.5)Si-(0.5-2)Al-(0-0.5)Cr (wt%) steels could achieve the 3G AHSS mechanical property targets and be successfully galvanized. The fabrication of thus Medium-Mn steel is detailed by (Pallisco and McDermid, 2020).

Table 1 Chemistry of Steel M in wt%

Steel ID	C	Mn	Si	Al	Cr
M	0.15	5.8	0.7	1.8	0.04

Prototype Medium-Mn steel (Steel M) with a 80%M-20%F (MF) starting microstructure was first obtained by annealing at 890°C for 10 min followed by an IA at 3 different temperatures (IATs of 665/685/710°C) for 120s.

This narrow temperature range was chosen based on pervious works done on a similar steel which showed dramatic variability in TRIP kinetics[3].

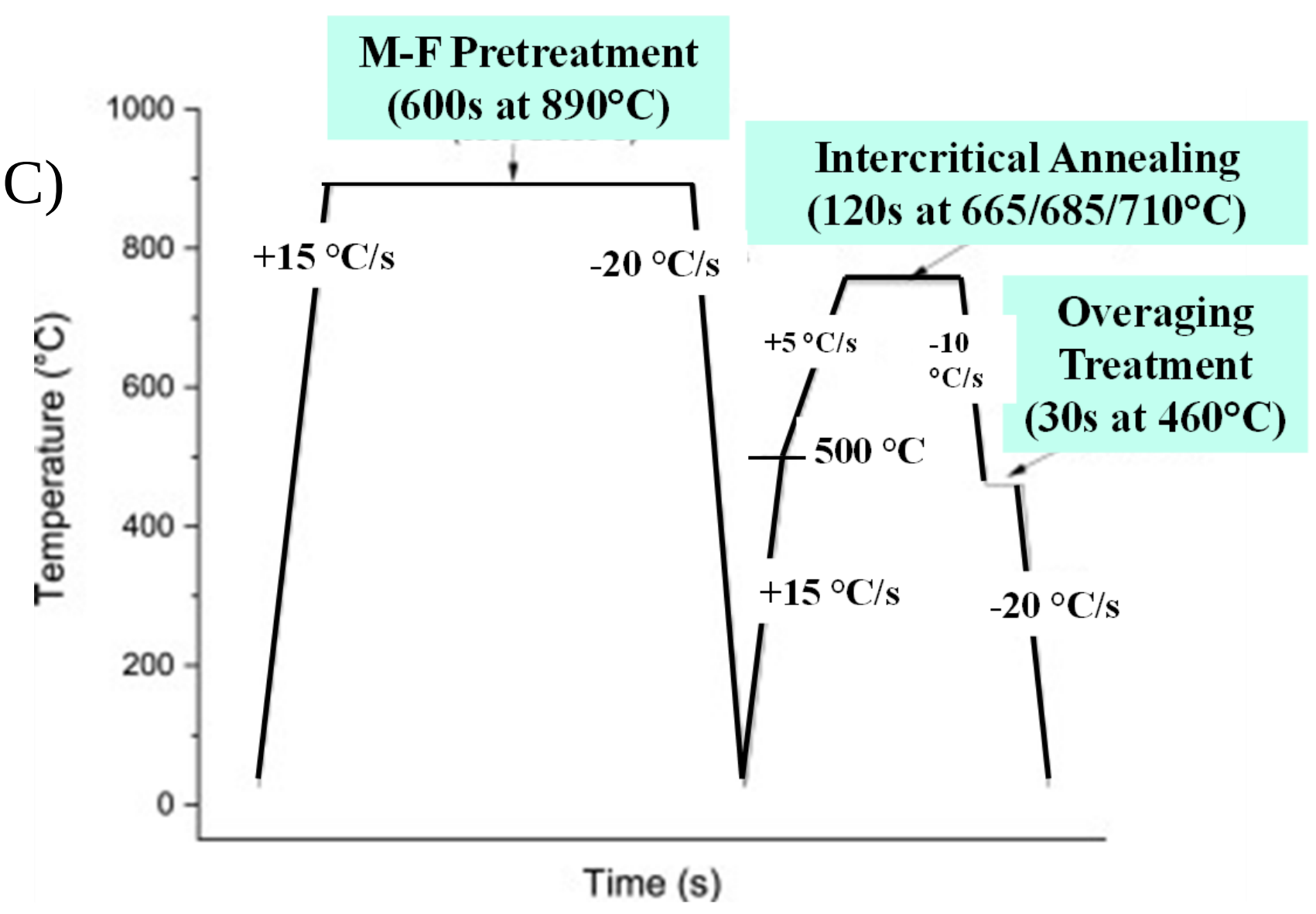

Figure 3 Thermal Profile for experimental IA treatments

Experimental Techniques

In-situ SEM Tensile Testing Coupled with μDIC

Hourglass-shaped tensile specimens were electropolished at 20V in a -20ºC liquid-nitrogen-cooled 10% perchloric solution in methanol. Electropolishing of this multiphase Medium-Mn steel resulted in excellent EBSD indexing and sufficient grey scale variation for Digital Image Correlation (DIC) post-processing. This enabled the micro-strain tracking of phases, particularly RA, on the material's surface as a function of increasing local average strain.

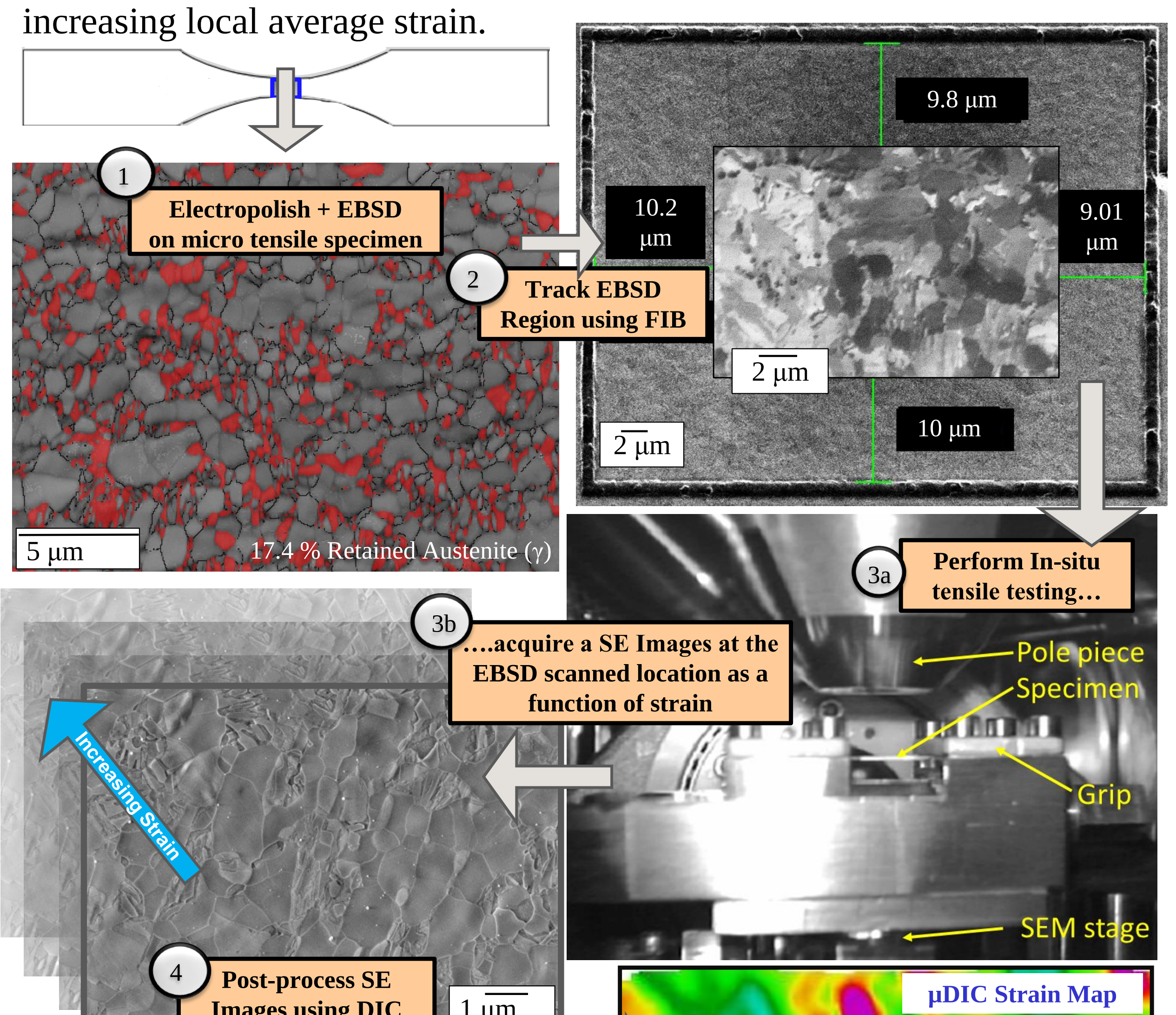

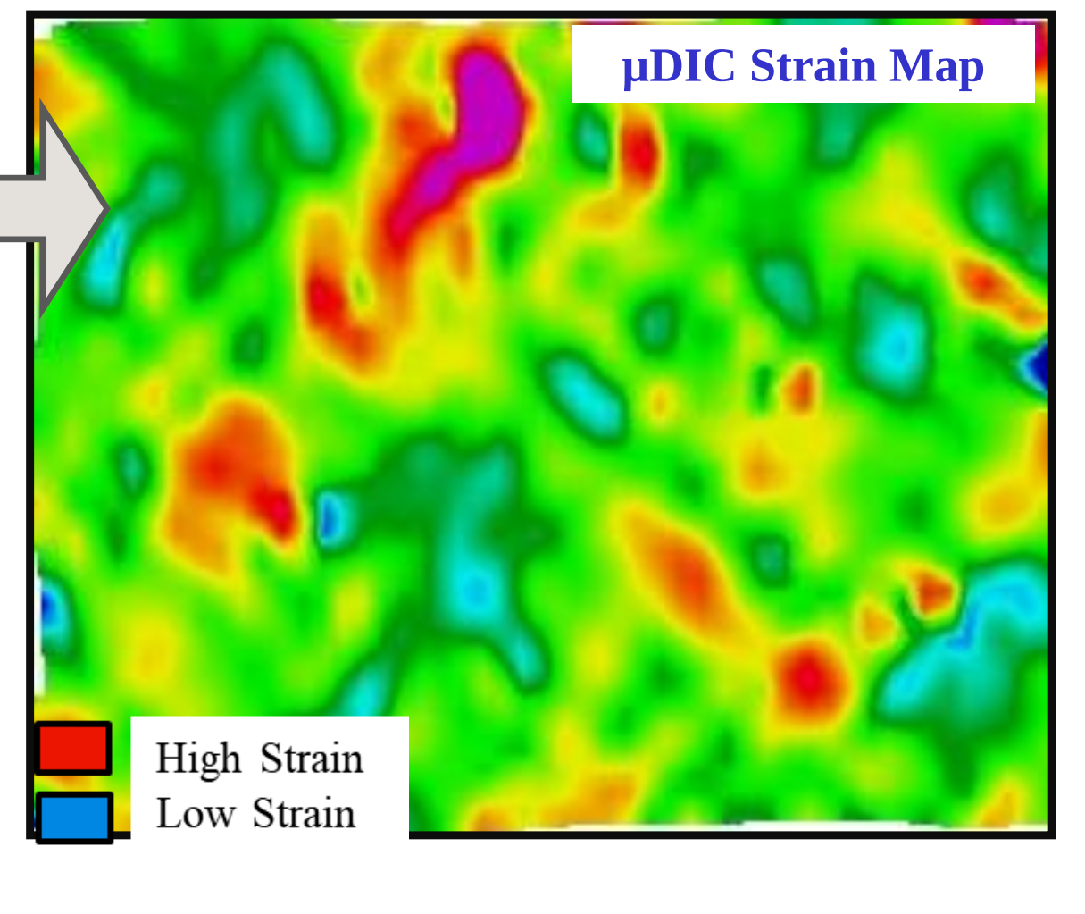

An in-lens detector in a field emission gun (JSM-7000-FEG) SEM was used to obtain high resolution images at high magnifications. The use of a manual in-house built tensile stage allows the working distance to be decreased. Strains were computed using ARAMIS©

X-ray microtomography

A Bruker Skyscan1172 desktop X-ray microtomography (μXCT) scanner equipped with a 100kV x-ray source and an Al/Cu filter at the highest resolution possible (0.7μm/pxl) was used in this study.

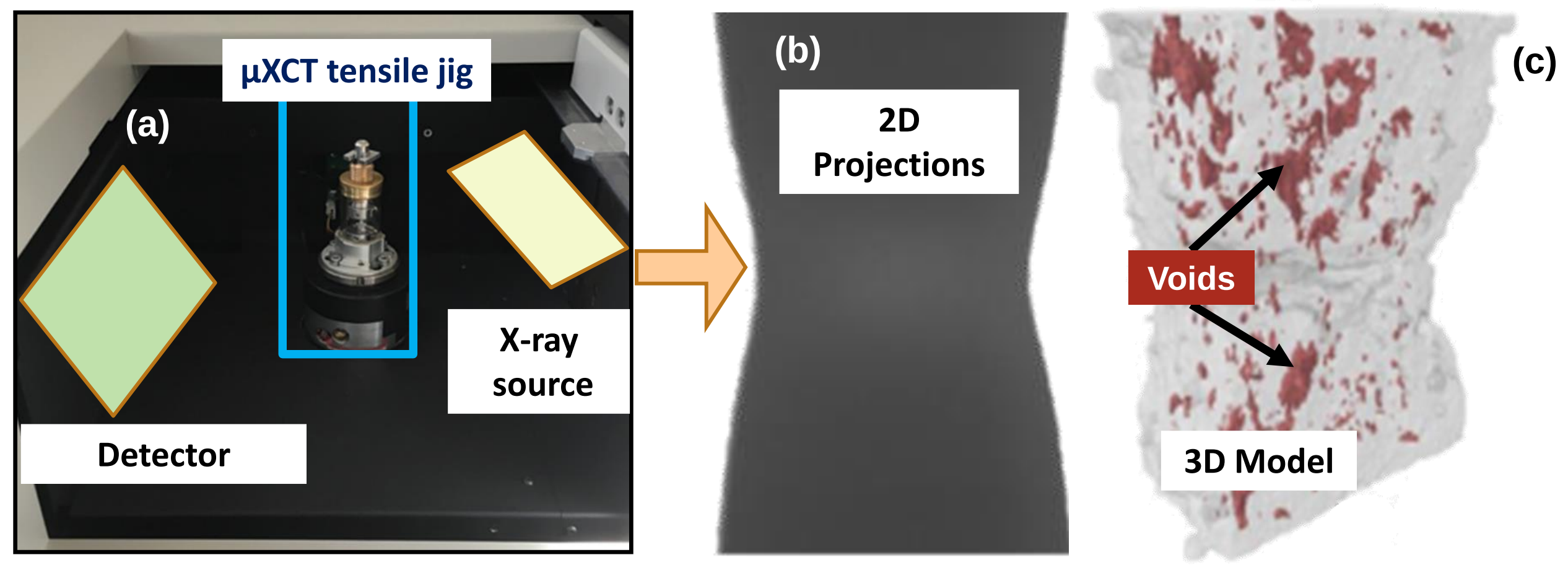

Figure 4 (a) Set Up of μXCT (b) 2D Projections collected during scanning (c) 3D modelling of Voids within the specimen

Results & Discussion

Mechanical Properties & TRIP Kinetics

Standardized tensile testing and interrupted tensile tests coupled with XRD using sub-size ASTM E8[4] samples were used to determine the tensile properties and TRIP kinetics of Steel M with a MF starting microstructure from IATs 665/685/710ºC for 120s

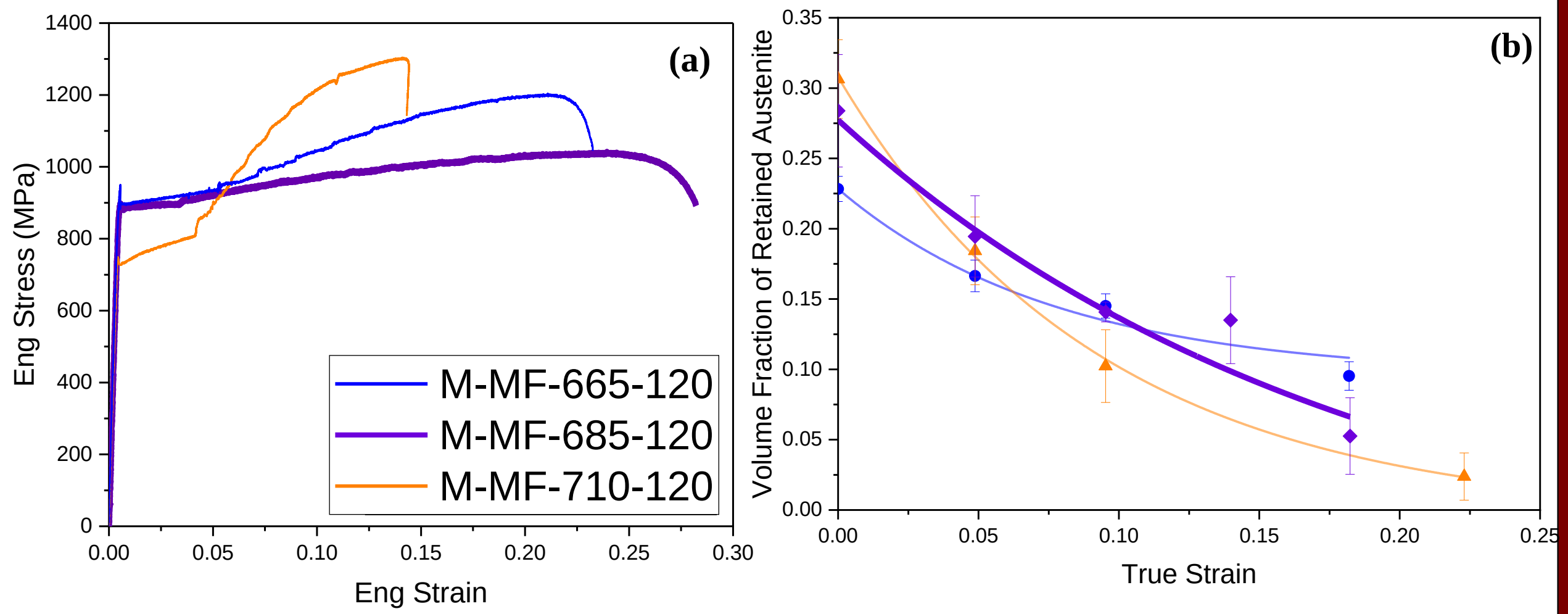

Figure 5 (a) Engineering Tensile Curves
(b) TRIP as a function of True Strain

Void Analysis

2D Analysis of fractured Steel M with a MF starting microstructure samples intercritically annealed from 665–710ºC for 120s and under different triaxial states of stress at the optimized IAT

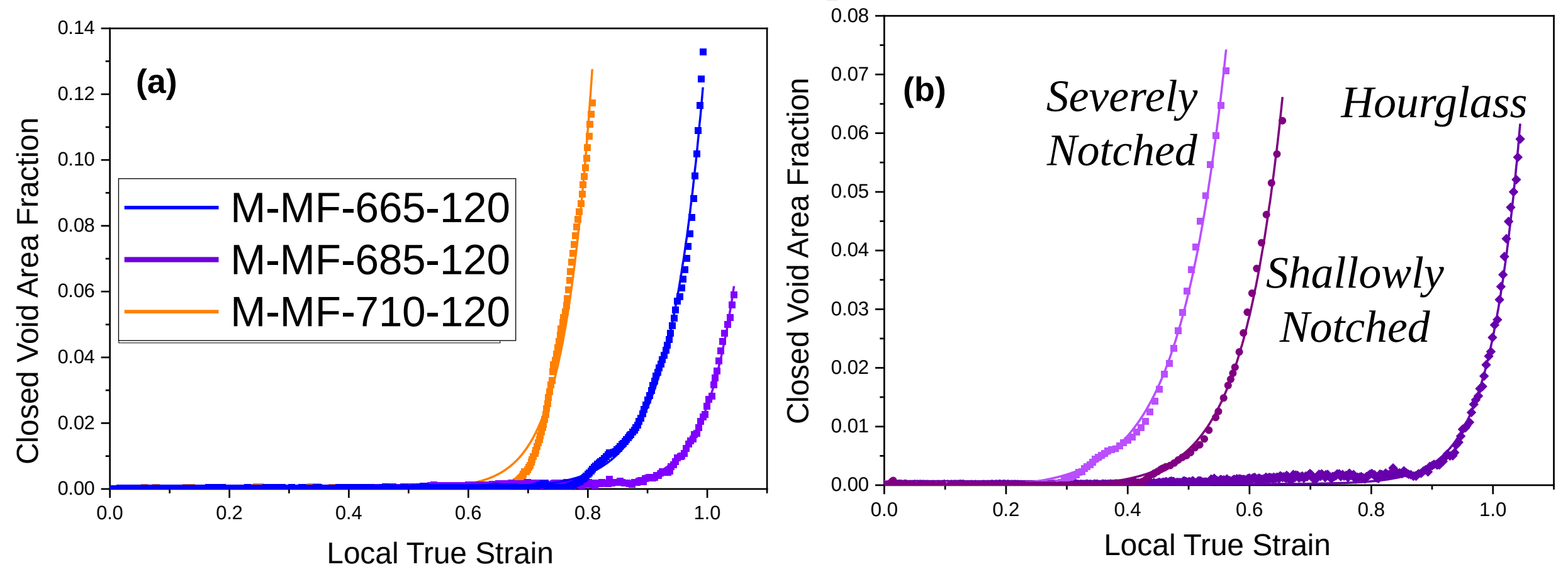

Figure 6 Closed Void Area fraction of (a) hourglass samples from IATs of 665–710 ºC
(b) Severely notched to hourglass samples at an IAT of 685 ºC

3D Analysis of 100-200 largest voids on fractured Steel M with a MF starting microstructure samples intercritically annealed at 665–710ºC for 120s and under different triaxial states of stress at the optimized IAT.

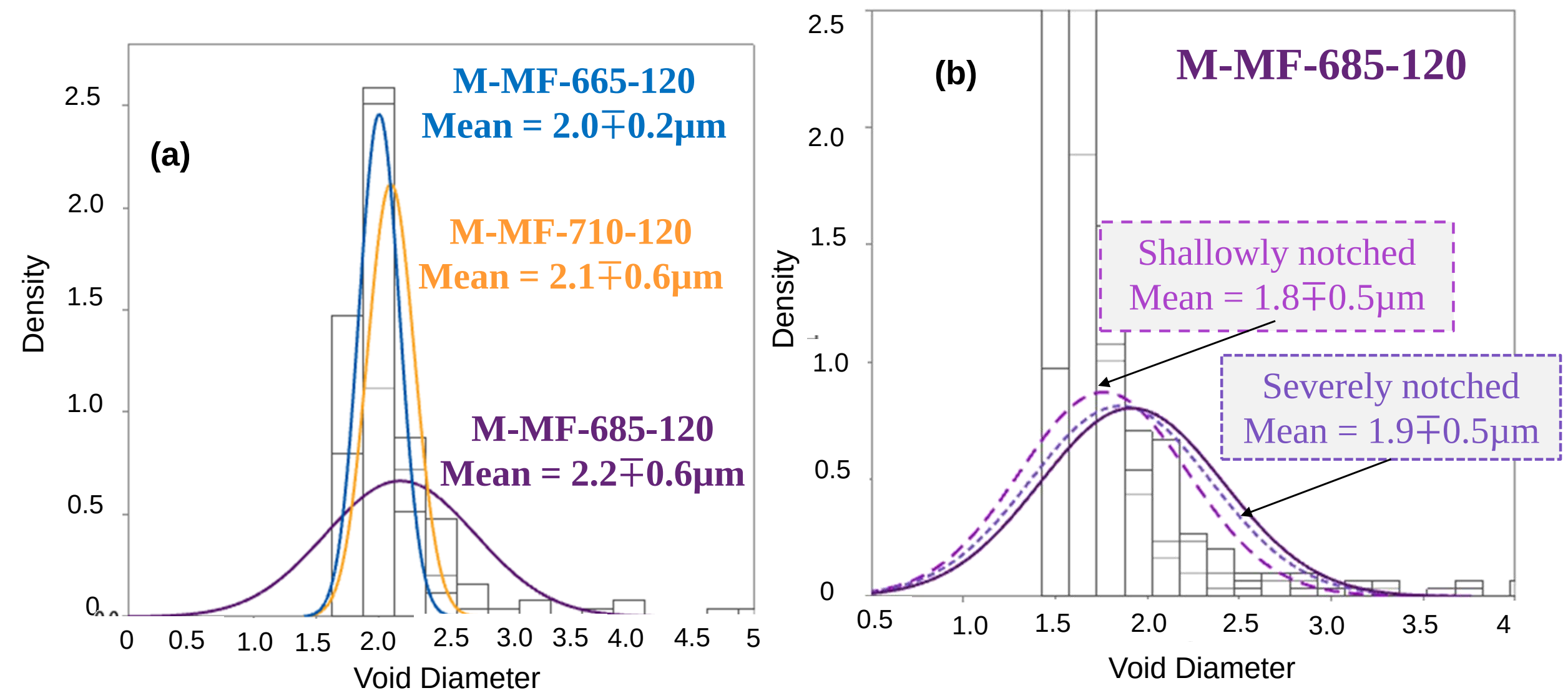

Figure 7 Void Diameters of (a) hourglass samples from IATs of 665–710ºC
(b) Severely notched to hourglass samples at an IAT of 685 ºC

Strain Partitioning of Phases

- In different triaxial stress states, the M/F regions shows greater deforming potential than RA regions
- The severely notched sample showed the least strain partitioning between M/F and RA phases

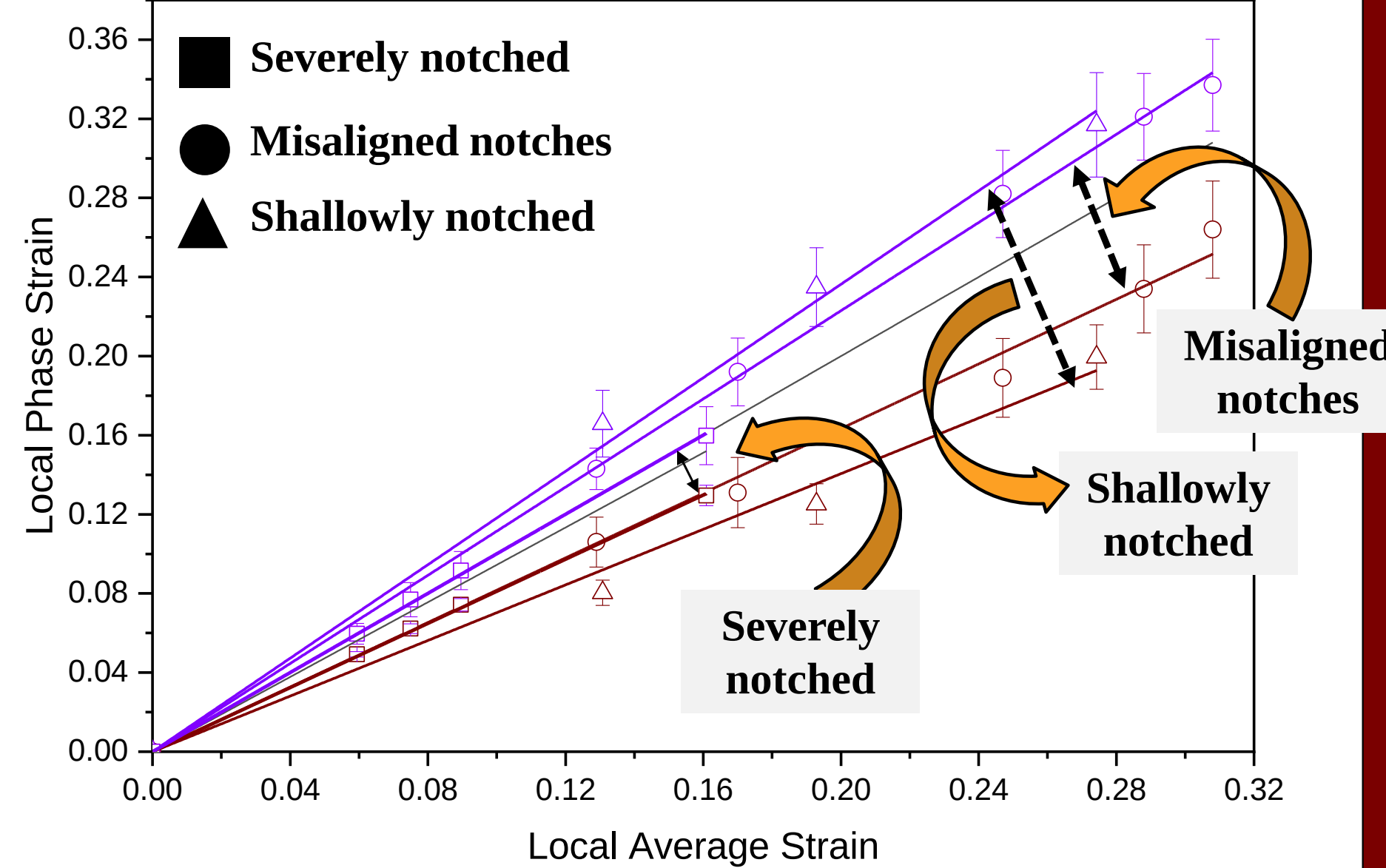

Figure 8 Strain Partitioning of M/F and RA regions under different triaxial states of stress

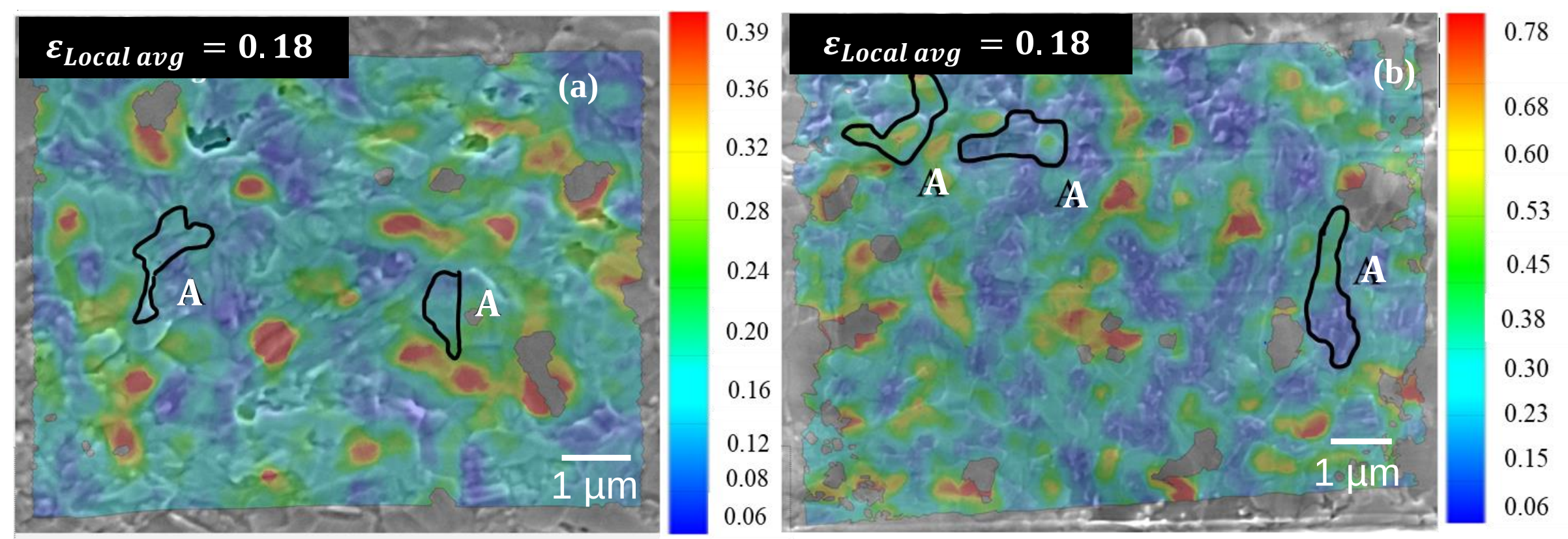

Figure 9 Traced Austenite regions on μDIC at high local average strains
(a) Severely Notched (b) Misaligned Notches

Conclusions

- Steel M with an MF starting microstructure intercritically annealed at 685°C for 120s showed the optimized damage-inducing condition with the least closed voids nucleated at fracture (in 2D) & greatest variability in void diameter size (in 3D)
- 3D Triaxiality investigations on the optimized IAT of 685°C showed voids growing to the same variability in diameter
- 2D Triaxiality investigations on the optimized IAT of 685°C condition showed the M/F regions to be deforming more than the RA regions in the microstructure

Major Future Work

- Post-process recently acquired volumetric austenite measurements unnotched and notched specimens to superimpose on damage evolution μXCT curves of Medium-Mn steels. Exemplifying the result in Figure 10.

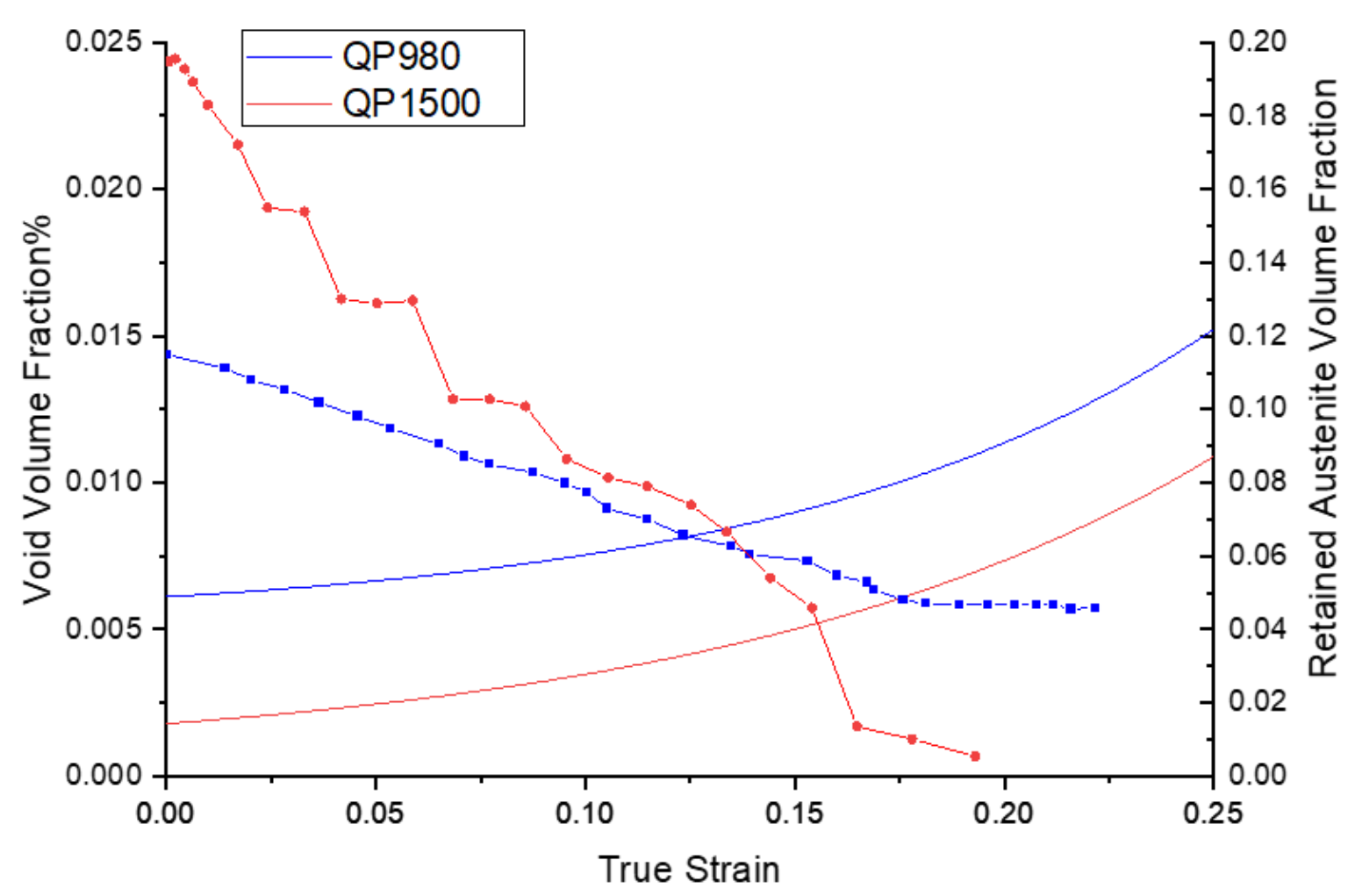

Figure 10 Volumetric Austenite measurements & damage evolution curves as a function of strain of 3G Quench & Partition (Q&P) steels[5,6]

Acknowledgements

We gratefully acknowledge the financial support of NSERC (grant CRDPJ 522309-17) and the IZA-GAP members. U.S. Steel R&D is gratefully acknowledged for their in-kind fabrication of the experimental steels.

References

1. Datsko, J. & Yang, C. T. Correlation of Bendability of Materials With Their Tensile Properties. *J. Eng. Ind.* 309–313 (1960).
2. Hance, B. Advanced high strength steel: Deciphering local and global formability. *Int. Automot. Body Congr. IABC 2016 DEARBORN - Pap.* (2016).
3. Pallisco, D. M. & McDermid, J. R. Mechanical property development of a 0.15C–6Mn–2Al–1Si third-generation advanced high strength steel using continuous galvanizing heat treatments. *Mater. Sci. Eng. A* 778, 139111 (2020).
4. ASTM E8/E8M – 21. Standard Test Methods for Tension Testing of Metallic Materials. *ASTM International* (2021).
5. Hu, X. H., Sun, X., Hector, L. G. & Ren, Y. Individual phase constitutive properties of a TRIP-assisted QP980 steel from a combined synchrotron X-ray diffraction and crystal plasticity approach. *Acta Mater.* 132, 230–244 (2017).
6. Samei, J., Pelligra, C., Amirmaleki, M. & Wilkinson, D. S. Microstructural design for damage tolerance in high strength steels. *Mater. Lett.* 269, (2020).